

Robust superconductivity near constant temperature in rubidium-doped C_{60}

Li-Na Zong,^{1,*} Ren-Shu Wang,^{2,1,*} Di Peng,¹ and Xiao-Jia Chen^{1,2,†}

¹*Center for High Pressure Science and Technology Advanced Research, Shanghai 201203, China*

²*School of Science, Harbin Institute of Technology, Shenzhen 518055, China*

(Dated: August 9, 2022)

To establish the doping-dependent phase diagram in alkali-metal doped C_{60} , we synthesize Rb-doped C_{60} samples with different stoichiometries by using the improved wet-chemistry technique. The doping levels determined from the Raman scattering spectra often show the appearance of three electrons corresponding to the band filling of three for the synthesized compounds no matter what dopants are used. The multiple phase coexistence with the unique Rb_3C_{60} is identified from the refined x-ray diffraction patterns. The phase fraction of Rb_3C_{60} is found to behave with the doping in a similar manner as the superconducting shielding fraction. These rigorously established correlations among the superconducting transition temperature along with the structural and phonon vibrational properties allow us to single out Rb_3C_{60} as the only superconducting phase with the nearly constant transition temperature regardless the doping level. These findings provide an experimental constraint on the theory developments for the superconductivity in fullerenes.

The discovery of superconductivity in alkali-metal doped C_{60} has stimulated great interest in exploring the chemical and physical properties of these amazing molecular superconductors. Within one year, the critical temperature (T_c) of fullerene superconductors has been raised from 18 to 33 K [1–3]; till now, the highest record of T_c at about 40 K has been achieved in Cs-doped C_{60} under pressure [4–7]. In the early stage, it has been discovered that T_c is in a linear relation with the lattice parameter of alkali-metal doped fullerenes [8–10], ascribing the family to conventional BCS superconductors, in which T_c is primarily tuned by the density of states at Fermi level. Chemical and physical pressure are two prevalent methods of tuning such a parameter in alkali fullerenes, and numerous works have been reported in this area [10–13]. Besides, tuning carrier concentration is another method to affect the state of states but has failed in the exploration for K-doped and Rb-doped binary C_{60} [11, 14]. Interestingly, such a correlation between T_c and carrier concentration was established in two cubic fullerenes, $Na_2Cs_xC_{60}$ and $M_{3-y}Ba_yC_{60}$ ($M = K, Rb, \text{ or } Cs$) [15]. A peaked T_c was observed at or very near the half-filling of t_{1u} band ($n = 3$) in these compounds with the decreasing tendency on either side, resembling the evolution of T_c with hole doping in cuprates [16], which cannot be explained within the conventional BCS theory but can be well reproduced if the electron-electron and electron-phonon interactions are treated on an equal footing by using the dynamical mean-field theory [17]. The cooperation of the electron-phonon coupling and the electron correlations has been increasingly focused and explored since the discovery of the dome-like evolution of T_c with pressure in Cs-doped fullerenes [5, 7, 18, 19].

Experimentally, the controversies remain regarding whether A_3C_{60} ($A=K, Rb, Cs$) is the single superconducting phase in alkali-metal doped fullerenes [20–22] or T_c changes with the doping level x in a parabolic way in A_xC_{60} . For K (Rb)-doped C_{60} , it has been found

that the T_c does not change with increasing alkali metal doping composition x [11, 14]. For Li_xCsC_{60} fullerenes, T_c was reported to change with variable t_{1u} band filling, which also shows a similar electron doping dependence of T_c as reported in two cubic fullerenes [23]. For K-doped C_{60} films, the effect of the carrier concentration on T_c was also reported [24]. Nevertheless, it is still doubtful whether the valence state dependence of T_c is a general rule in fullerene superconductors or not. Rb-doped C_{60} is the second reported superconductor in this family, which shows the highest T_c of 28–29 K at ambient pressure in binary compounds [2]. Previous works on x-ray diffraction and Raman spectroscopy measurements demonstrate that nonstoichiometric Rb intercalation can be realized in this compound [25, 26]. Thus, we choose Rb-doped C_{60} to examine the evolution of T_c with Rb doping concentrations and try to establish the correlations among T_c , crystal structure, and charge transfer in these compounds.

The high-quality of our synthesized samples of Rb-doped C_{60} is demonstrated by the successful realization of both the Meissner effect and zero-resistance state from the dc [Figs. 2(a)–2(g)] and ac [Fig. 2(h)] susceptibility (χ) as well as resistivity [Fig. 2(i)] measurements. The imaginary part of the susceptibility (χ'') [Fig. 2(h)] is correlated with the energy dissipation due to the formation of superconducting vortex current. A single sharp peak in χ'' can be considered as a qualitative criterion for the realization of the zero-resistance state [27], in good agreement with the resistivity data collected on the same sample as shown in Fig. 2(i). It should be mentioned that the identification of superconductivity from both the Meissner effect and zero-resistance state on the same sample rather than different ones was only completed recently for K-doped [28, 29] and Rb-doped [30] C_{60} after the improvement of the synthesis technique. The early experiments for providing evidence of superconductivity either from the Meissner effect [2, 3] or the

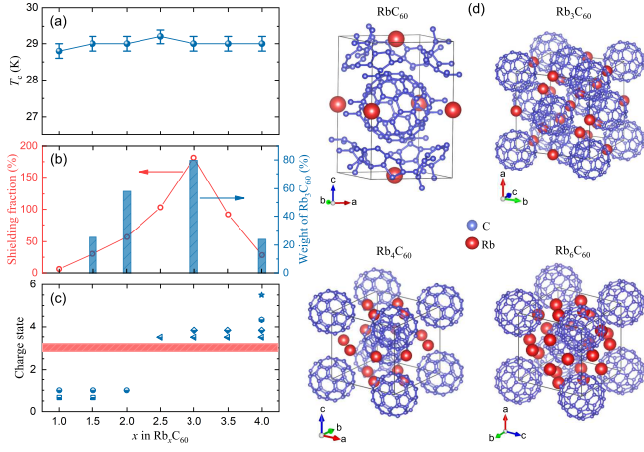


FIG. 1: (Color online) Superconducting phases in Rb_xC_{60} with different stoichiometries. (a) The evolution of T_c with doping x . Error bars represent the estimated uncertainties. (b) Left axis: Plot of the superconducting shielding fraction as a function of x . Right axis: The phase fraction of Rb_3C_{60} in the studied samples ($x = 1.5, 2.0, 3.0$, and 4.0) obtained from x-ray diffraction analysis. (c) The evolution of charge state with x . The shaded region highlights the common charge state in all studied compositions. (d) Schematic crystal structure of Rb_xC_{60} ($x=1, 3, 4$, and 6). The violet and red spheres represent C and Rb atoms, respectively.

zero-resistance state [31, 32] or rarely from both but on the different samples [1]. So far, the essential evidence for superconductivity from the zero-resistance state for Cs_3C_{60} is still missing and waits to be filled up [4–7]. Holding the two essential characters of superconductivity for Rb-doped C_{60} make this study confident in examining the doping effect on superconductivity compared to the early studies [15, 23].

Our central results for Rb_xC_{60} with different stoichiometries are summarized in Fig. 1. Based on the magnetization measurements, as shown in Fig. 1(a), T_c resists doping concentrations within our studied stoichiometric range. The similar phenomenon was observed previously but with only a few compositions [11]. In Fig. 1(b), the regularity obtained from the magnetization measurements for a series of samples is that the shielding fraction reaches a maximum in nominal Rb_3C_{60} and decreases on either side of $x = 3$. This phenomenon was also noticed for K-doped C_{60} and Rb-doped C_{60} [11, 14], indicating that the superconducting phase in these compounds is close to $x = 3$ but still lack of unambiguous evidence. According to the x-ray diffraction analysis, the right axis of Fig. 1(b) displays the phase fraction of the refined Rb_3C_{60} in nominal $\text{Rb}_{1.5}\text{C}_{60}$, Rb_2C_{60} , Rb_3C_{60} , and Rb_4C_{60} . The change of the phase fraction for refined Rb_3C_{60} with increasing Rb concentration is analogous to the law established for shielding fraction, namely, the phase fraction of Rb_3C_{60} is peaked at nominal composition $x = 3$ and also decreases on either side. Apart

from that, based on the refinement results, we also find that, at room temperature, there are 4 stable phases in Rb_xC_{60} within our studied scope, including RbC_{60} , Rb_3C_{60} , Rb_4C_{60} , and Rb_6C_{60} , whose structure can be assigned to the orthorhombic, face-centered cubic (*f.c.c.*), body-centered tetragonal (*b.c.t.*), and body-centered cubic (*b.c.c.*) phase, respectively. Figure 1(d) exhibits the schematic crystal structures for the phases mentioned above, which are in accord with those reported in Ref. [33]. Based on the Raman scattering measurements, Fig. 1(c) depicts the overall evolution of the charge state of C_{60} with increasing Rb doping concentration. Different charge states can be detected in one sample, which suggests that phase separation is a common feature for Rb_xC_{60} . In addition, the charge state of C_{60} increases gradually with increasing doping composition, in which the phase with 3 charge transfer is the common phase in all compositions. Combining the results derived from the magnetization, x-ray diffraction, and Raman spectroscopy measurements, one can safely draw a conclusion that the robust superconductivity with T_c of 28–29 K resisting doping concentrations in Rb-doped C_{60} is from *f.c.c.* Rb_3C_{60} with exact 3 charge transfer. Besides, phase separation is verified by both x-ray diffraction and Raman spectroscopy in all the studied Rb-doped C_{60} .

The shown T_c and superconducting shielding fraction for each Rb_xC_{60} in Figs. 1(a) and 1(b) (left axis) are based on the *dc* magnetization measurements. Figure 2(a)-2(g) show the temperature dependence of *dc* χ for samples with different nominal compositions. Both the zero-field-cooling run (ZFC, blue curve) and the field-cooling run (FC, red curve) for each sample exhibit obvious diamagnetic transition, in which the ZFC and the FC runs represent the magnetic exclusion and the magnetic expulsion, respectively. The big difference between two curves is a phenomenon of flux trapping, which is a typical character of type-II superconductors. Particularly, the ZFC curve and the FC curve for nominal RbC_{60} show anomalous features after the superconducting transition. The ZFC curve has a small paramagnetic bump, and the FC curve flips into weak-paramagnetic area. This phenomenon has also been observed in other work [34], in which it was attributed to the systematic error caused by remanent field in the instrument, but it also may be derived from the strong flux-pinning caused by large amounts of defects or non-superconducting phases. Due to the sonication treatment in the synthesis method, polycrystalline powders are inclined to form, and the granular effect is so distinct that the superconducting transition is not narrow enough for our samples. Thus, a defining method of T_c having been applied for powdered samples is adopted to give an accurate result [34]. The inset of each figure shows an expanded view near the superconducting transition and presents the method to determine T_c for each sample. The critical temperature is defined as the first temperature point that devi-

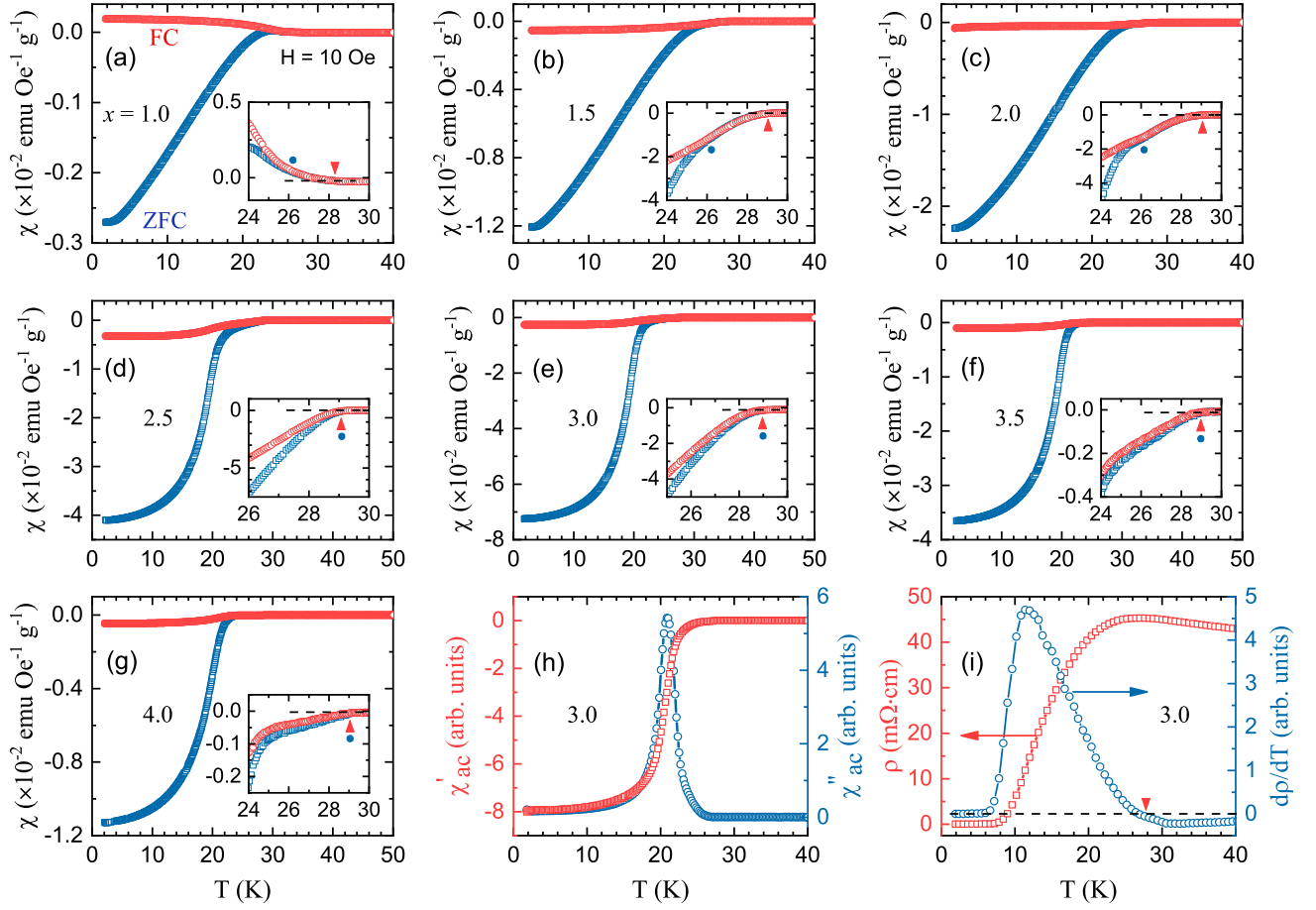


FIG. 2: (Color online) Superconductivity in nominal Rb_xC_{60} ($x=1, 1.5, 2, 2.5, 3, 3.5$, and 4). (a)-(g) Temperature dependence of the dc χ . Inset: An expanded view in a narrow temperature range near the superconducting transition. The dashed lines represent the linear extrapolation from the normal state (30 K), and the temperatures marked by solid triangles and solid circles for each sample represent the real T_c and the branching point for the ZFC and FC curves, respectively. (h) Temperature dependence of the ac χ for nominal Rb_3C_{60} . (i) Temperature dependence of the electrical resistivity (ρ) and its derivative for nominal Rb_3C_{60} .

ates from the linear extrapolation of the normal state, as marked by a solid triangle in each inset. This temperature represents the initial point for the formation of electron pairs. Such a definition gives the consistent T_c value for Rb_3C_{60} as indicated from the dc [Fig. 2(e)] and ac χ [Fig. 2(h)] together with resistivity [Fig. 2(i)] measurements on the same sample. For nominal RbC_{60} , $\text{Rb}_{1.5}\text{C}_{60}$, and Rb_2C_{60} compounds, the T_c is not consistent with the branching point of the ZFC and FC curves marked by the solid circle, which may result from the deteriorated superconducting phase. Assuming the density (δ) of our synthesized samples is 2 g cm^{-3} , one can calculate the superconducting shielding fraction ($\text{SF} = 4\pi\chi\delta$) by using the magnetic susceptibility collected at 2 K with an applied field of 10 Oe. The obtained results are displayed in Fig. 1(b). For nominal $\text{Rb}_{2.5}\text{C}_{60}$ and Rb_3C_{60} , the apparent SF is larger than 100%, which has also been discovered in previous K- and Rb-doped C_{60} superconductors [35, 36]. For type-II superconductors,

the SF is usually larger than the superconducting volume fraction, and the former is also in proportion to the latter; only in perfect superconductors, the SF is equal to the superconducting fraction and can be calculated in terms of the FC susceptibility [37]. Due to the demagnetization factor, the SF could be larger than 100%, and it is a normal phenomenon in alkali-metal doped C_{60} .

The shown phase fraction of Rb_3C_{60} [right axis of Fig. 1(b)] and the crystal structures [Fig. 1(d)] of the synthesized samples were determined from the well refined x-ray diffraction data for nominal Rb_xC_{60} ($x=1.5, 2, 3$, and 4). Figure 3 displays the Rietveld refinement results for each sample. The detailed refinement results including the phase fraction, space group, and lattice parameters are given in Table I. As learned, phase separation is a common feature, and all samples have at least two phases, in which nominal $\text{Rb}_{1.5}\text{C}_{60}$, Rb_2C_{60} , and Rb_3C_{60} have two coexisting phases, and nominal Rb_4C_{60} has three coexisting phases. With increasing Rb doping concentra-

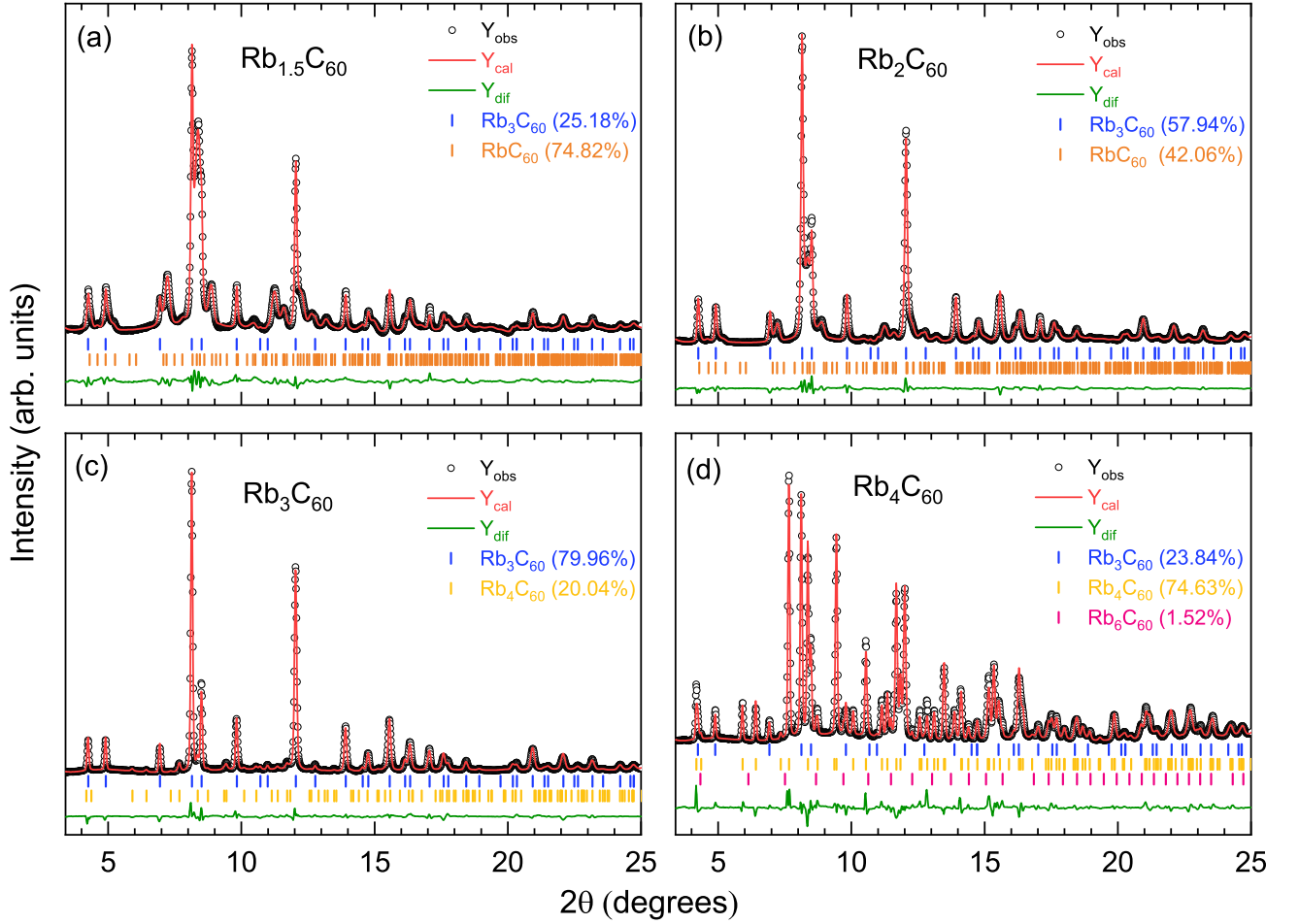


FIG. 3: (Color online) (a)-(d) X-ray diffraction spectra and Rietveld refinements of Rb_xC_{60} ($x=1.5, 2, 3$, and 4). Experimentally observed (open circles), calculated (red lines), and difference profiles (dark green lines) of the multi-phase refinement are given for each sample. Sticks represent the calculated reflection positions for different phases.

tion, different phases with variable Rb compositions appear. In nominal $\text{Rb}_{1.5}\text{C}_{60}$ and Rb_2C_{60} , the orthorhombic RbC_{60} in the space group of $Pmnn$ coexists with the *f.c.c.* Rb_3C_{60} with the space group of $Fm\bar{3}m$. In nominal Rb_3C_{60} and Rb_4C_{60} , the *f.c.c.* Rb_3C_{60} coexists with the *b.c.t.* Rb_4C_{60} with the space group of $I4/mmm$, but traces of *b.c.c.* Rb_6C_{60} in the space group of $Im\bar{3}$ can also be detected in nominal Rb_4C_{60} . The *f.c.c.* Rb_3C_{60} is the common phase in all studied samples, whose phase fraction is peaked at nominal composition $x = 3$, as shown in Fig. 1(b). Figure 1(d) displays the crystal structure for the four phases mentioned above. The *f.c.c.* Rb_3C_{60} is the most studied phase and the generally-accepted superconducting phase [22, 38]. The crystal structure of Rb_4C_{60} resembles that for Rb_6C_{60} but losing two Rb atoms on the four faces parallel to the *c* axis, and it can be regarded as a distorted *b.c.c.* structure.

The charge state of the phase with increasing Rb concentration shown in Fig. 1(c) was determined from the analysis of the collected Raman spectra (Fig. 4). As

shown in Fig. 4(a), for pristine C_{60} , there are six obvious Raman active modes, consisting of four radial H_g modes and two tangential A_g modes. Upon increasing electron doping, the downshift of the $A_g(2)$ mode for one electron is 6 cm^{-1} , consistent with the charge transfer law [39, 40]. For the phases with charge state (n) ≤ 1 , there are six apparent Raman active modes like those in pristine C_{60} , but the relative intensity between the $H_g(1)$ [$A_g(1)$] mode and $A_g(2)$ mode increases apparently upon doping. Apart from that, the broadened line width for the $H_g(7)$ and $H_g(8)$ modes is another character for charge transfer as reported in previous works [41], indicating the increased electron-phonon coupling. For the phase with exact 3 charge transfer, only 4 Raman active modes can be detected on the spectra, including the two low-energy H_g modes and two high-energy A_g modes. The most prominent feature for this state is the increasingly broadened $H_g(1)$ and $H_g(2)$ modes, which is generally recognized as a character of strong electron-phonon coupling [42]. The characters detected from our

TABLE I: Rietveld refinement results of the phase and its weight w (in %) with the space group (sg), lattice parameter(s) (in Å), unit cell volume V (in Å³), weighted profile R -factor (R_{wp} in %), and goodness of fit (Gof in %) for nominal Rb_xC_{60} ($x=1.5, 2, 3$, and 4).

x	w (sg)	a, b, c	V	R_{wp}	Gof
1.5	RbC ₆₀ -74.82 ($Pmnn$)	$a=9.1297(64)$ $b=10.0495(63)$ $c=14.483(10)$	1328.8(16)	7.698	0.729
	Rb ₃ C ₆₀ -25.18 ($Fm\bar{3}m$)	$a=14.4823(65)$	3037.0(31)		
2	RbC ₆₀ -42.06 ($Pmnn$)	$a=9.0342(62)$ $b=10.0841(73)$ $c=14.480(12)$	1319.2(17)	5.730	0.718
	Rb ₃ C ₆₀ -57.94 ($Fm\bar{3}m$)	$a=14.4616(67)$	3024.3(31)		
3	Rb ₃ C ₆₀ -79.96 ($Fm\bar{3}m$)	$a=14.4755(71)$	3032.9(33)	8.104	1.150
	Rb ₄ C ₆₀ -20.04 ($I4/mmm$)	$a=12.0256(66)$ $c=11.0380(66)$	1596.3(20)		
4	Rb ₃ C ₆₀ -23.84 ($Fm\bar{3}m$)	$a=14.5162(79)$	3060.8(38)	10.776	1.336
	Rb ₄ C ₆₀ -74.63 ($I4/mmm$)	$a=12.0162(63)$ $c=11.0826(58)$	1600.2(19)		
	Rb ₆ C ₆₀ -1.52 ($Im\bar{3}$)	$a=11.5898(63)$	1556.8(25)		

spectra are consistent with those reported for Rb₃C₆₀ [42]. It is well accepted that the phase with 3 charge transfer or half-filling t_{1u} band is in a metallic state and can be attributed to the superconducting phase of alkali-fullerides [43]. When the charge transfer is larger than 3, the Raman active modes are similar to those with $n = 3$. The gradually narrowed $H_g(1)$ and $H_g(2)$ modes have the strong salient features, which is reminiscent of the spectra for Rb₄C₆₀ [44]. The largest charge state of 5.5 corresponds to an early stage of the fully-doped Rb₆C₆₀, which has also been reported in K-doped C₆₀ [45]. In particular, the phase with $n = 5.5$ observed at one point in nominal Rb₄C₆₀ is only a coexisting phase for another one with less charge transfer ($n = 3.5$), which also indicates that only traces of Rb₆C₆₀ can be detected in nominal Rb₄C₆₀. This result is consistent with the phase fraction of Rb₆C₆₀ obtained from the x-ray diffraction analysis. Similar to the XRD data, phase separation is a prominent character for our Rb-doped C₆₀ compounds. However, the charge state of three electrons is the only feature shared for all the doped compounds. Therefore, the corresponding Rb₃C₆₀ is identified as the only phase to exhibit superconductivity with nearly constant T_c upon the change of Rb concentration. This comprehensive study fails to find the desired dome shape for the T_c change with doping in Rb-doped C₆₀ and hopes to provide the base on the theory development of superconductivity in fullerides.

Experimental details: Pristine C₆₀ (> 99.5%) were purchased from Tokyo Chemical Industry (Shanghai) and used without further purification. The rubidium metal with purity no less than 99.75% was purchased from Alfa Aesar. We adopted a similar wet-chemical method to synthesize Rb-doped C₆₀ samples with different compositions as that in our previous work [30]. The pre-weighted C₆₀ (40 mg) and rubidium metal with different mole ratio (C₆₀ : Rb = 1:1.0-4.0) were first put in a borosilicate vial, and then 3-4 mL ultra-dry tetrahydrofuran solvent was poured into the vial. After that, the reaction vial sealed with a cap was transferred to an ultrasonic instrument with oil bath and was sonicated for 9-10 minutes at about 40 °C. After sonication, the colorless solvent turned into dark-purple or red-brown mixtures, which depended on the mole ratio of Rb metal, and then the reaction vial was loaded on a vortex oscillator and further reacted for 6-8 h before a still standing process. After the standing process, the precipitated product was filtrated and a black precursor with solvent molecules was obtained. For samples with nominal stoichiometry in the range of 1.0-2.0, due to the high solubility of the synthesized samples, no precipitation could be obtained by the standing process. N-hexane, as a precipitation agent, was added to accelerate the precipitation and to acquire a highly crystallized sample. Annealing process was conducted at 220 °C for 48 hours in an inert atmosphere followed by a natural cooling process. All the manipulations mentioned above were carried out in a glovebox filled with argon (99.999%) and with the content of H₂O and O₂ less than 0.1 ppm.

After obtaining the final products, they were sealed in non-magnetic capsules and glass capillary tubes for magnetization, Raman spectroscopy, and Synchrotron x-ray diffraction measurements, respectively. The magnetization measurements were performed in a SQUID magnetometer (Quantum Design) with a given magnetic field of 10 Oe. Both dc and ac magnetic susceptibility were collected to give an overall magnetic behavior. In dc magnetic susceptibility measurements, the sample was first cooled down to 2 K, and then a magnetic field of 10 Oe was applied, zero-field-cooling data were recorded while warming to 40 or 50 K. The field-cooling run was collected at the same magnetic field when the sample was cooled down to 2 K again. For the dc magnetic susceptibility measurements, the probe magnetic amplitude and frequency are 1 Oe and 234 Hz, respectively. The resistivity for nominal Rb₃C₆₀ was also obtained by applying a dc four-probe method in Van Der Pauw configuration [46] in the Physical Properties Measurement System (Quantum Design). Raman spectroscopy was collected in an in-house system with a charged coupled device and spectrometer from Princeton Instruments. The laser with a wavelength of 488 nm and laser power less than 1 mW was adopted to avoid the possible radiation damage. The integration time for each spectrum was set

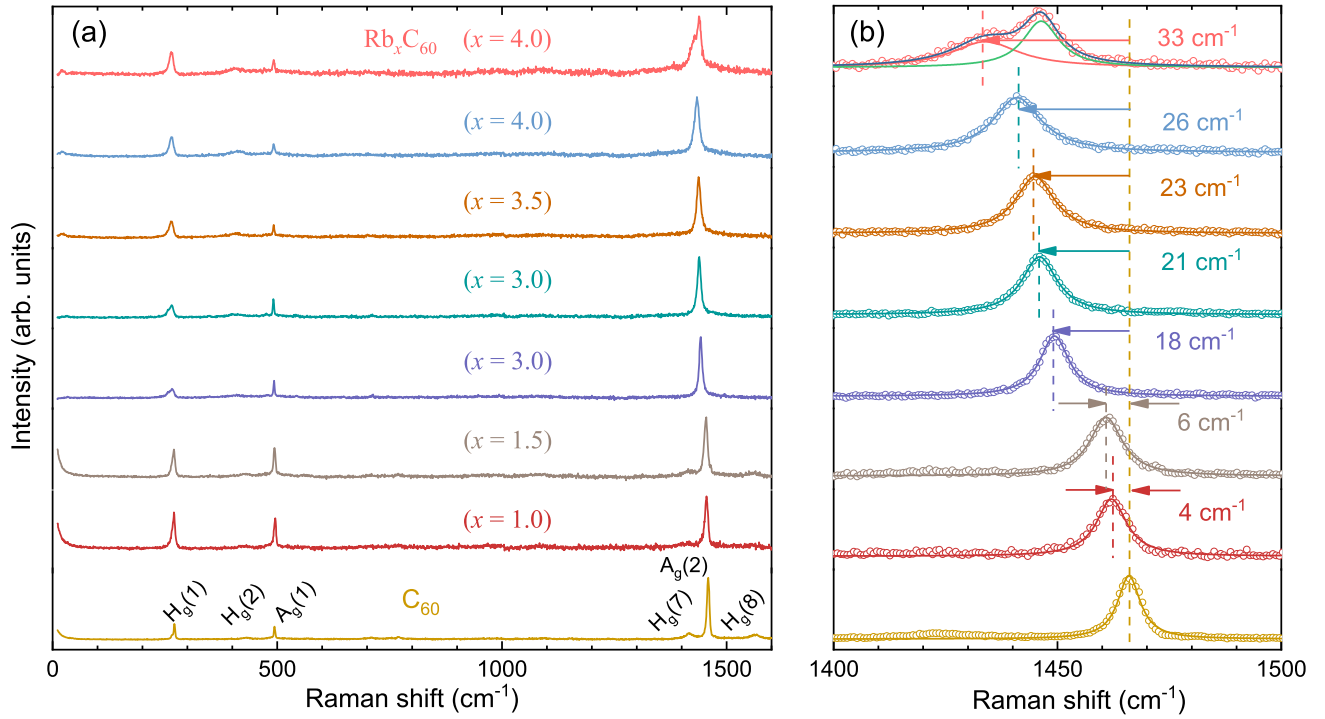


FIG. 4: (Color online) Raman spectra in the full range (a) and the expanded view of the $A_g(2)$ modes (b) of pristine C_{60} and Rb-doped C_{60} with increasing charge transfer. The hollow circles represent the observed profiles, and the solid lines are the Lorentz fitting results.

to 1 min. To give an accurate result, all Raman spectra were collected under the same conditions, and we collected 5-7 spectra from different points in one sample to ensure the comparability between data. Synchrotron x-ray diffraction patterns were collected on the BL15U1 synchrotron beamline at Shanghai Synchrotron Research Facility using a focused monochromatic beam. An incident x-ray beam with wavelength of 0.6199 Å and a Mar165 two-dimensional charge-coupled device detector were used in the measurement. The obtained XRD patterns were integrated and analyzed in Dioptas software package [47]. The standard Rietveld refinement was performed to get the knowledge of the space group, the unit cell parameters, and the phase fractions for different co-existing phases using Topas software package [48].

This work was funded by the Shenzhen Science and Technology Program (Grant No. KQTD20200820113045081), the Basic Research Program of Shenzhen (Grant No. JCYJ20200109112810241), and the National Key R&D Program of China (Grant No. 2018YFA0305900).

* These authors contributed equally to this work

† Electronic address: xjchen2@gmail.com

[1] A. F. Hebard, M. J. Rosseinsky, R. C. Haddon, D. W. Murphy, S. H. Glarum, T. T. M. Palstra, A. P. Ramirez,

and A. R. Kortan, *Nature* **350**, 600 (1991).

[2] M. J. Rosseinsky, A. P. Ramirez, S. H. Glarum, D. W. Murphy, R. C. Haddon, A. F. Hebard, T. T. M. Palstra, A. R. Kortan, S. M. Zahurak, and A. V. Makhija, *Phys. Rev. Lett.* **66**, 2830 (1991).

[3] K. Tanigaki, T. W. Ebbesen, S. Saito, J. Mizuki, J. S. Tsai, Y. Kubo, and S. Kuroshima, *Nature* **352**, 222 (1991).

[4] T. T. M. Palstra, O. Zhou, Y. Iwasa, P. E. Sulewski, R. M. Fleming, and B. R. Zegarski, *Solid State Commun.* **93**, 327 (1995).

[5] A. Y. Ganin, Y. Takabayashi, Y. Z. Khimyak, S. Margadonna, A. Tamai, M. J. Rosseinsky, and K. Prassides, *Nat. Mater.* **7**, 367 (2008).

[6] Y. Takabayashi, A. Y. Ganin, P. Jeglič, D. Arčon, T. Takano, Y. Iwasa, Y. Ohishi, M. Takata, N. Takeshita, K. Prassides, and M. J. Rosseinsky, *Science* **323**, 1585 (2009).

[7] A. Y. Ganin, Y. Takabayashi, P. Jeglič, D. Arčon, A. Potočnik, P. J. Baker, Y. Ohishi, M. T. McDonald, M. D. Tzirakis, A. McLennan, G. R. Darling, M. Takata, M. J. Rosseinsky, and K. Prassides, *Nature* **466**, 221 (2010).

[8] R. M. Fleming, A. P. Ramirez, M. J. Rosseinsky, D. W. Murphy, R. C. Haddon, S. M. Zahurak, and A. V. Makhija, *Nature* **352**, 787 (1991).

[9] O. Zhou, G. B. M. Vaughan, Q. Zhu, J. E. Fischer, P. A. Heiney, N. Coustel, J. P. McCauley, Jr., and A. B. Smith III, *Science* **255**, 833 (1992).

[10] T. Yildirim, J. E. Fischer, R. Dinnebier, P. W. Stephens, and C. L. Lin, *Solid State Commun.* **93**, 269 (1995).

[11] C. C. Chen, S. P. Kelty, and C. M. Lieber, *Science* **253**, 886 (1991).

- [12] K. Tanigaki, I. Hirosawa, T. W. Ebbesen, J. Mizuki, Y. Shimakawa, Y. Kubo, J. S. Tsai, and S. Kuroshima, *Nature* **356**, 419 (1992).
- [13] G. Sparn, J. D. Thompson, R. L. Whetten, S.-M. Huang, R. B. Kaner, and F. Diederich, *Phys. Rev. Lett.* **68**, 1228 (1992).
- [14] K. Holczer, O. Klein, S. M. Huang, R. B. Kaner, K. J. Fu, F. Whetten, R. L. Diederich, and F. Diederich, *Science* **252**, 1154 (1991).
- [15] T. Yildirim, L. Barbedette, J. E. Fischer, C. L. Lin, J. Robert, P. Petit, and T. T. M. Palstra, *Phys. Rev. Lett.* **77**, 167 (1996).
- [16] B. Keimer, S. A. Kivelson, M. R. Norman, S. Uchida, and J. Zaanen, *Nature* **518**, 179 (2015).
- [17] J. E. Han, O. Gunnarsson, and V. H. Crespi, *Phys. Rev. Lett.* **90**, 167006 (2003).
- [18] M. Capone, M. Fabrizio, C. Castellani, and E. Tosatti, *Science* **296**, 2364 (2002).
- [19] R. H. Zadik, Y. Takabayashi, G. Klupp, R. H. Colman, A. Y. Ganin, A. Potočník, P. Jeglič, D. Arčon, P. Matus, K. Kamarás, Y. Kasahara, Y. Iwasa, A. N. Fitch, Y. Ohishi, G. Garbarino, K. Kato, M. J. Rosseinsky, and K. Prassides, *Sci. Adv.* **1**, 1500059 (2015).
- [20] P. W. Stephens, L. Mihaly, P. L. Lee, R. L. Whetten, S. M. Huang, R. Kaner, F. Diederich, and K. Holczer, *Nature* **351**, 632 (1991).
- [21] D. W. Murphy, M. J. Rosseinsky, R. M. Fleming, R. Tycko, A. P. Ramirez, R. C. Haddon, T. Siegrist, G. Dabbagh, J. C. Tully, and R. E. Walstedt, *J. Phys. Chem. Solids* **53**, 1321 (1992).
- [22] J. E. Fischer, G. Bendele, R. Dinnebier, P. W. Stephens, C. L. Lin, N. Bykovetz, and Q. Zhu, *J. Phys. Chem. Solids* **56**, 1445 (1995).
- [23] M. Kosaka, K. Tanigaki, K. Prassides, S. Margadonna, A. Lappas, C. M. Brown, and A. N. Fitch, *Phys. Rev. B* **59**, R6628 (1999).
- [24] M. Q. Ren, S. Han, S. Z. Wang, J. Q. Fan, C. L. Song, X. C. Ma, and Q. K. Xue, *Phys. Rev. Lett.* **124**, 187001 (2020).
- [25] Q. Zhu, O. Zhou, N. Coustel, G. B. M. Vaughan, J. P. McCauley, Jr, W. J. Romanow, J. E. Fischer, and A. B. Smith III, *Science* **254**, 545 (1991).
- [26] M. G. Mitch, S. J. Chase, and J. S. Lannin, *Phys. Rev. Lett.* **68**, 883 (1992).
- [27] F. Gömöry, *Supercond. Sci. Technol.* **10**, 523 (1997).
- [28] R. S. Wang, D. Peng, J. W. Hu, L. N. Zong, and X. J. Chen, *Carbon* **195**, 1 (2022).
- [29] R. S. Wang, D. Peng, L. N. Zong, L. C. Chen, and X. J. Chen, *Carbon* (<https://doi.org/10.1016/j.carbon.2022.07.070>) (2022).
- [30] L. N. Zong, R. S. Wang, D. Peng, and X. J. Chen, *J. Phys. Chem. C* **126**, 2912 (2022).
- [31] T. T. M. Palstra, R. C. Haddon, A. F. Hebard, and J. Zaanen, *Phys. Rev. Lett.* **68**, 1054 (1992).
- [32] Y. Maruyama, T. Inabe, H. Ogata, Y. Achiba, S. Suzuki, K. Kikuchi, and I. Ikemoto, *Chem. Lett.* **20**, 1849 (1991).
- [33] R. M. Fleming, M. J. Rosseinsky, A. P. Ramirez, D. W. Murphy, J. C. Tully, R. C. Haddon, T. Siegrist, R. Tycko, S. H. Glarum, P. Marsh, G. Dabbagh, S. M. Zahurak, A. V. Makhija, and C. Hampton, *Nature* **352**, 701 (1991).
- [34] P. Dahlke, M. S. Denning, P. F. Henry, and M. J. Rosseinsky, *J. Am. Chem. Soc.* **122**, 12352 (2000).
- [35] S. H. Irons, J. Z. Liu, P. Klavins, and R. N. Shelton, *Phys. Rev. B* **52**, 15517 (1995).
- [36] V. Buntar, F. M. Sauerzopf, H. W. Weber, M. Halushka, and H. Kuzmany, *Phys. Rev. B* **72**, 024521 (2005).
- [37] V. Buntar and H. W. Weber, *Supercond. Sci. Technol.* **9**, 599 (1996).
- [38] J. P. McCauley, Jr., Q. Zhu, N. Coustel, O. Zhou, G. Vaughan, S. H. J. Idziak, J. E. Fischer, S. W. Tozer, D. M. Groski, N. Bykovetz, C. L. Lin, A. R. McGhie, B. H. Allen, W. J. Romanow, A. M. Denenstein, and A. B. Smith III, *J. Am. Chem. Soc.* **113**, 8537 (1991).
- [39] R. C. Haddon, A. F. Hebard, M. J. Rosseinsky, D. W. Murphy, S. J. Duclos, K. B. Lyons, B. Miller, J. M. Rosamilia, R. M. Fleming, A. R. Kortan, S. H. Glarum, A. V. Makhija, A. J. Muller, R. H. Eick, S. M. Zahurak, R. Tycko, G. Dabbagh, and F. A. Thiel, *Nature* **350**, 320 (1991).
- [40] H. Kuzmany, M. Matus, B. Burger, and J. Winter, *Adv. Mater.* **6**, 731 (1994).
- [41] J. Winter and H. Kuzmany, *Phys. Rev. B* **52**, 7115 (1995).
- [42] P. Zhou, K. A. Wang, P. C. Eklund, G. Dresselhaus, and M. S. Dresselhaus, *Phys. Rev. B* **48**, 8412 (1993).
- [43] R. C. Haddon, *Acc. Chem. Res.* **25**, 127 (1992).
- [44] M. G. Mitch and J. S. Lannin, *Phys. Rev. B* **51**, 6784 (1995).
- [45] J. Winter and H. Kuzmany, *Solid State Commun.* **84**, 935 (1992).
- [46] L. J. Van der Pauw, *Philips Res. Rep.* **13**, 1 (1958).
- [47] C. Prescher and V. B. Prakapenka, *High Press. Res.* **35**, 223 (2015).
- [48] A. A. Coelho, *J. Appl. Cryst.* **51**, 210 (2018).